**Climate
of the Past**
Open Access
Discussions

A two thousand year annual record of snow accumulation rates for Law Dome, East Antarctica

J. Roberts[1,2], C. Plummer[2,3], T. Vance[2], T. van Ommen[1,2], A. Moy[1,2], S. Poynter[2], A. Treverrow[2], M. Curran[1,2], and S. George[2]

[1]Australian Antarctic Division, Kingston, Tasmania 7050, Australia
[2]Antarctic Climate & Ecosystems Cooperative Research Centre, University of Tasmania, Hobart, Tasmania 7001, Australia
[3]Institute for Marine and Antarctic Studies, University of Tasmania, Hobart, Tasmania 7001, Australia

CPD

10, 4469–4497, 2014

Law Dome accumulation

J. Roberts et al.

Title Page

Abstract	Introduction
Conclusions	References
Tables	Figures

|◄ | ►|
◄ | ►
Back | Close

Full Screen / Esc

Printer-friendly Version

Interactive Discussion

Abstract

Accurate high resolution records of snow accumulation rates in Antarctica are crucial for estimating ice sheet mass balance and subsequent sea level change. Snowfall rates at Law Dome, East Antarctica, have been linked with regional atmospheric circulation to mid-latitudes as well as regional Antarctic snowfall. Here, we extend the Law Dome accumulation record from 750 to 2035 years, using recent annual layer dating that extends to AD –22. Accumulation rates were calculated as the ratio of measured to modelled layer thicknesses, multiplied by the long term mean accumulation rate. The modelled layer thicknesses were based on a power law vertical strain rate profile fitted to observed annual layer thickness. The periods AD 380–442, AD 727–783 and AD 1970–2009 have above average snow accumulation rates, while AD 663–704, AD 933–975 and AD 1429–1468 were below average. The calculated snow accumulation rates show good correlation with atmospheric reanalysis estimates, and significant spatial correlation over a wide expanse of East Antarctica, demonstrating that the Law Dome record captures larger scale variability across a large region of East Antarctica well beyond the immediate vicinity of the Law Dome summit. Spectral analysis reveals periodicities in the snow accumulation record which may be related to ENSO and Interdecadal Pacific Oscillation frequencies.

1 Introduction

The short and sparse instrumental record in the high latitudes of the Southern Hemisphere means investigating long-term precipitation variability in this region is difficult without access to suitable proxy records. Antarctic ice core data can provide suitable local measurements for annual precipitation. However, in order to derive accurate snow accumulation rates, snowfall must be high enough to resolve annual layering in the presence of deposition noise due to surface processes, and layer thinning from ice flow and snow densification must be suitably constrained.

Furthermore, the annual layering records the net input of snow at the site and includes the annual snow accumulation rate, the loss through ablation and the transport of wind blown surface snow. Due to the lack of melt and relatively low winds at the ice-coring site, evaporation and wind losses are expected to make a minor contribution to long term variability and are neglected.

Law Dome (Fig. 1) is a small independent icecap in East Antarctica (Morgan et al., 1997) with a maritime climate yielding sufficiently high snow accumulation rates to allow annual layer resolution to AD −22. Law Dome is separated from the submarine-based Aurora Subglacial Basin (Roberts et al., 2011) by the Vanderford trench and associated Totten and Vanderford glacier systems. Consequently, ice flow at Law Dome is largely independent of the East Antarctic ice sheet and orography results in a strong East–West snow accumulation gradient (Morgan et al., 1997).

The principal ice core from Law Dome is the Dome Summit South (DSS) core (66.7697° S, 112.8069° E, 1370 m elevation) which was drilled approximately 4.6 km SSW of the dome summit (Morgan et al., 1997) between 1987 and 1992. This site was selected for its favourable bedrock topography and sufficiently low surface temperatures (mean annual average of −21.8 °C) to preclude summer melt (Morgan et al., 1997). The annual snow accumulation rate at DSS is $0.68\,\mathrm{m\,yr^{-1}}$ ice equivalent ($\mathrm{m\,yr^{-1}}$ ie) (van Ommen et al., 2004, where an ice density of $917\,\mathrm{kg\,m^{-3}}$ is used to convert between $\mathrm{kg\,m^{-2}\,yr^{-1}}$ of water and the ice equivalent), allowing sub-annual resolution of water stable isotopes and trace ions. The DSS record has been updated incrementally with short cores drilled in subsequent years providing a complete 2035-year record spanning AD −22 to AD 2012.

Coastal Antarctic ice core records with high resolution are being used increasingly to reconstruct specific aspects of Southern Hemisphere climate. For example, climate modes such the Southern Annular Mode (SAM), the El Niño-Southern Oscillation (ENSO) and the Interdecadal Pacific Oscillation (IPO) have been reconstructed using annual layer-counted ice core records from Law Dome and elsewhere (Vance et al., 2013, 2014; Abram et al., 2014). Additionally, Law Dome has provided rainfall proxies

for both eastern Australia (Vance et al., 2013) (1000 years) and southwest Western Australia (van Ommen and Morgan, 2010) (750 years). The southwest Western Australian (SWWA) rainfall proxy occurs via a direct precipitation oscillation between Law Dome and SWWA, as a result of spatially-coherent, meridional wind patterns that push cool-dry or warm-moist air to either Law Dome or SWWA. The precipitation oscillation has been related to long-term variability in the zonal wave-number three (ZW3) pattern, injecting a meridional component to the dominant westerly wind stream in the Southern Hemisphere (Raphael, 2004; van Ommen and Morgan, 2010).

This study extends the Law Dome annual snow accumulation rate record from 750 years (van Ommen and Morgan, 2010) to greater than 2000 years and increases the instrumental overlap (and therefore calibration) period by 7 years (or 26 %) to span AD 1979–2012.

2   Law Dome ice cores

Four ice cores from the Dome Summit South (DSS) site at Law Dome were used to construct a composite snow accumulation rate record. The main DSS core (DSS-main) is augmented in the upper portion by three other ice cores: DSS1213, DSS97 and DSS99. DSS1213 covers the recent epoch AD 1989–2012, while DSS97 and DSS99 are used for intermediate data in the epochs AD 1888–1988 and AD 1841–1887 respectively. DSS97 and DSS99 replace sections of the upper part of the DSS-main core that were subject to poor core quality, due to a combination of melt infiltration from thermal drilling in firn and drill performance issues in the changeover to electromechanical drilling deeper down. This composite record extends a previous composite compiled from a series of short overlapping firn cores drilled in 2001, 2008 and 2009 (Plummer et al., 2012) and shows good replication with stable isotope signals during the period of overlap with the previous record.

The upper section of the DSS composite ice core record is dated by identifying annual layers in the seasonally-varying water stable isotope ratios (δ^{18}O and δD).

Annual boundaries are defined by the peak of the summer isotope maximum, which has been identified as occurring on average around 10 January (van Ommen and Morgan, 1997). The isotope layer counting is verified by seasonally-varying trace ions to a depth of 796.138 m, which corresponds to AD −22. Dating error is small; ±1 years after AD 894 and reaches a maximum uncertainty of +4/ − 7 years at AD −22, which reflects ambiguities in the interpretation of the record (Plummer et al., 2012). The uncertainty estimate allows AD −22 to be a maximum 7 years older or 4 years younger than dated.

All depths (except Fig. 2) and annual layer thicknesses are reported as ice equivalent depth (z), measured downward from the ice surface and calculated from the physical depth (z') using,

$$z = \int_0^{z'} \rho(\eta)\,d\eta \tag{1}$$

where the density profile, $\rho(\eta)$, is based on an empirical fit to the DSS-main core measurements (van Ommen et al., 2004). Time independence of the density profile (Sorge's Law, Patterson, 1994) is confirmed by the close correspondence between the density profiles from DSS-main and DSS1213 (separated in time by 15 years), as shown in Fig. 2.

3 Accumulation history

As firn is advected deeper into the ice sheet due to burial by subsequent snowfall and the bulk downward and outward flow of the ice sheet, the annual layers thin as a result of the vertical velocity gradient (the vertical strain rate). This thinning can be mathematically modelled and a correction factor applied if the vertical strain rate profile is known or can be estimated. A correction was applied to the composite record using coefficients modelled from the DSS-main core, which provided more robust estimates

than the shorter records as the extra length damps the influence of short-duration fluctuations.

Ice thinning is modelled by applying a calculated vertical strain rate profile to a layer of initial thickness equal to the long-term average annual snow accumulation rate. The actual snow accumulation rate for any year (and corresponding depth) is then estimated as the ratio of the actual annual layer thickness relative to the modelled layer thickness multiplied by the long-term average annual snow accumulation rate.

$$a(t) = a \cdot \frac{z(t)}{Z(t)} \tag{2}$$

where $a(t)$ is the annual snow accumulation rate for year t, a is the long term annual snow accumulation rate, $z(t)$ is the observed annual layer thickness for year t and $Z(t)$ is the corresponding modelled annual layer thickness based on the long term annual snow accumulation rate and the vertical strain rate profile. This method assumes that any change in layer thickness is due only to the vertical strain, and that there is no long-term trend in snow accumulation rate.

Two accumulation histories, each corrected using a different vertical strain profile are compared. The vertical strain rate models used are (i) a piece-wise linear model (Dansgaard and Johnsen, 1969) and (ii) a power law model (Lliboutry, 1979).

3.1 Piece-wise linear vertical strain rate model

The effects of layer thinning due to vertical strain rate can be accounted for by linear least squares fitting of a Dansgaard and Johnsen (1969) model to the ice equivalent annual layer thickness data as a function of ice equivalent depth. This model has two distinct regions; a lower region with a linear increase in vertical strain rate from zero at the base of the ice sheet, and an overlying region of constant vertical strain rate. Integration of such a strain rate profile yields a vertical velocity profile with corresponding quadratic and linear segments. Previous modelling of the layer thinning for the DSS-main core (Morgan et al., 1997) using a Dansgaard and Johnsen relation

Full Screen / Esc

Printer-friendly Version

Interactive Discussion

places the transition between these regions at a depth of 839 m ie (ice-equivalent), somewhat below the 774 m ie maximum depth of the composite record in this study. Consequently, the annual layer thickness model requires just two free parameters: the long-term annual snow accumulation rate and the constant vertical strain rate.

The long-term average snow accumulation rate calculated from the layer thickness model applied to the DSS-main core is $0.680 \pm 4.0 \times 10^{-3}$ (1 standard error) m yr^{-1} ie and the vertical strain rate is $6.32 \times 10^{-4} \pm 7.8 \times 10^{-6}$ yr^{-1}. The fit to the annual layer thickness data is shown in Fig. 3 and the snow accumulation rate time-series in Fig. 4a. A smoothed snow accumulation rate time-series using a Gaussian low-pass filter with width $\sigma = 2.99$ years (equivalent half power width 10 years) is also shown.

3.2 Power law vertical strain rate model

The piece-wise linear model assumes that in areas near ice divides and dome summits the vertical strain rate depth-profile is proportional to the horizontal velocity profile. This can be approximated by a linear lower segment and a constant upper segment (Dansgaard and Johnsen, 1969; Patterson, 1994). The depth-profile of horizontal ice velocity at the DSS site was determined by repeat measurements of the borehole inclination following ice core drilling (Morgan et al., 1998). Fitting a power law distribution (Lliboutry, 1979) to these horizontal velocities provides the basis for an improved vertical strain rate profile. As the temperature at the base of the borehole is below the in situ freezing point, we ignore any terms representing melt or slip at the base of the ice sheet. The free parameters of the model are estimated by least squares fitting to the borehole displacements of Morgan et al. (1998). Data near the surface (depths less than 75 m) were excluded as the upper section of the borehole was thermally drilled, causing problems with the borehole inclination data.

At depths below 800 m, which is beyond the zone of interest for the present study, the flow regime at DSS becomes more complex due to the influence of the surrounding bedrock topography. Additionally, deformation rates, particularly the simple shear strain rate, are increasingly influenced by the development of large-scale polycrystalline

anisotropy below 800 m (Morgan et al., 1998). In situations where ice flows over rough bedrock topography, the undisturbed flow in the upper portion of the ice sheet – that is relevant to the 2 kyr accumulation record – can be approximated by assuming flow over an offset smoothed surface above the true base (Hutter, 1982). The (virtual) origin of the velocity profile corresponding to the smoothed bed is also offset from the physical origin of the velocity profile at the bedrock.

The borehole horizontal displacement (D) is approximated by a power law profile with parameters determined from the model fit:

$$D = C \left(1 - \left(\frac{z}{H - z_0} \right)^p \right), \tag{3}$$

where z is the ice equivalent depth (m), $C = 4.35 \pm 3.8 \times 10^{-3}$ m is an arbitrary scaling factor, the exponent of the power law is $p = 4.19 \pm 0.025$ and $z_0 = 74.66 \pm 0.83$ m represents the (positive) vertical displacement of the virtual velocity profile origin. The constant $H = 1178.22$ m represents the approximate ice equivalent ice sheet thickness from the displacement data. The horizontal displacement and the derived power law are shown in Fig. 5.

Integrating Eq. (3) with respect to depth yields the vertical velocity profile $v(z)$

$$v(z) = a - sC \left(z - \frac{z}{p+1} \left(\frac{z}{H - z_0} \right)^p \right), \tag{4}$$

where a is the long-term annual snow accumulation rate (in m yr^{-1} ie) and s is a scaling factor linearly related to the modelled vertical strain rate at the surface.

A least squares optimisation of the resulting vertical velocity profile to the observed annual layer thicknesses for the DSS-main core yields a long-term average annual snow accumulation rate of $0.686 \pm 4.1 \times 10^{-3}$ m yr^{-1} ie and a surface vertical strain rate of $6.57 \times 10^{-4} \pm 8.1 \times 10^{-6}$, with the fit shown in Fig. 6. The resulting snow accumulation time-series, including a 10-year low-pass Gaussian filtered version, is shown in Fig. 4b.

Law Dome accumulation

J. Roberts et al.

|◀ | ▶|

| ◀ | ▶ |

| Back | Close |

Full Screen / Esc

Printer-friendly Version

Interactive Discussion

4 Discussion

The piece-wise linear vertical strain rate model assumes that flow near an ice divide is two-dimensional, so the vertical strain rate profile with depth is proportional to the longitudinal derivative of the horizontal velocity profile. As described previously, the horizontal velocity profile is approximated by a linear lower segment and a constant upper segment. While this may be a good approximation for sites where the flow is two-dimensional, the DSS site is located ~ 4 ice thicknesses (4.6 km) from the Law Dome summit where the flow is three-dimensional and slightly divergent (Morgan et al., 1998). Here, a power law approximation to the horizontal velocity profile is more realistic. A comparison of the modelled vertical strain rate profiles at DSS (Fig. 7) show that the piece-wise linear model generates higher vertical strain rates at depth. This leads to an underestimation of annual layer thicknesses at depth, and correspondingly higher snow accumulation rates.

Furthermore, the nature of the least squares fit required to calibrate the piece-wise linear model compensates for the excessive vertical strain rate at depth by lowering the constant strain rate in the upper region of the depth profile, producing a lower and potentially unrealistic estimate of layer thinning in this region. The result is a small negative trend in snow accumulation with depth in the upper part of the core, switching to a positive trend in the deeper parts. Overall, this produces a shallow concave bias in the snow accumulation rate estimates, with lower values at mid-depth (Fig. 4a).

Although we cannot exclude the possibility that this concave shape reflects a real environmental signal, we consider that the power law vertical strain rate profile provides a more realistic snow accumulation rate reconstruction at DSS through its connection with the observed horizontal displacement data.

The vertical strain rate magnitude at DSS is not solely related to the horizontal displacement profile, rather, it is dependent on the shape of the profile, due to the three-dimensional divergent nature of the DSS flow regime. The scaling parameter s (Eq. 4) accounts for the effects of three dimensional flow in the power law strain rate

model. Accordingly, we base the subsequent analyses on this model. Note, however, that the differences between the snow accumulation rate histories derived using the two vertical strain rate models are small ($< 0.04\,\mathrm{m\,yr^{-1}}$ ie for any year, see Fig. 4c) and the two records are in good agreement.

The shortcomings of the piece-wise linear vertical strain rate model, particularly for capturing variability on multi-centennial and shorter timescales, are further illustrated by comparing estimates of the vertical strain rate at the surface calculated using running 100 m subsets of the annual layer thickness data for each of the vertical strain rate models (Fig. 8). The vertical strain rates at the surface are more constant, and hence internally consistent, for the power law model. It should be noted that the results for both models are noisier in the upper portion of the ice-sheet (above ~ 400 m) and are not shown. This is driven by the significantly fewer annual data-points in 100 m intervals from this zone due to the reduced effects of layer thinning near the surface and imperfections in the density model.

The estimated vertical strain rate at the surface for the two models are in reasonable agreement ($6.32 \times 10^{-4} \pm 7.8 \times 10^{-6}\,\mathrm{yr^{-1}}$ compared to $6.57 \times 10^{-4} \pm 8.1 \times 10^{-6}\,\mathrm{yr^{-1}}$ for the piece-wise linear and power law models respectively). However, both of these values differ significantly from the surface GPS based value of $7.72 \times 10^{-4} \pm 3.1 \times 10^{-6}\,\mathrm{yr^{-1}}$ (Morgan et al., 1998). These differences might arise because the modelled vertical strain rates are estimated using data from only the upper portion of the ice sheet rather than the full ice sheet thickness.

The calculated long-term snow accumulation rate of $0.688 \pm 0.130\,\mathrm{m\,yr^{-1}}$ ie ($0.682 \pm 0.129\,\mathrm{m\,yr^{-1}}$ ie for the piece-wise linear model) is in close agreement with previous estimates of $0.678\,\mathrm{m\,yr^{-1}}$ ie (Morgan et al., 1997), $0.680\,\mathrm{m\,yr^{-1}}$ ie (van Ommen et al., 2004) and $0.688\,\mathrm{m\,yr^{-1}}$ ie (van Ommen and Morgan, 2010). The similarity of these estimates, each based on different, yet overlapping, epochs strongly suggests that either the assumption of no long-term trend in snow accumulation rate (see Sect. 3) is valid or that any trend in snow accumulation rate has been linear and constant over the last 2 kyr.

The snow accumulation rate distribution has a SD of 0.130 m yr⁻¹ ie and is slightly but significantly ($p < 0.001$, D'Agostino et al., 1990) positively skewed (0.47), i.e. it has a long tail at higher snow accumulation rates. Additionally, the distribution has more mass in the tails than a normal distribution, with a non-mesokurtic ($p < 0.001$, D'Agostino et al., 1990) probability density function, which specifically is leptokurtic, with slightly raised excess kurtosis (0.58).

The recent above-average snow accumulation rate period from AD 1970–2009 is the third largest in integrated snow accumulation excess throughout the record, after AD 380–442 and AD 727–783. However, it has the strongest anomaly as it occurs over a shorter time period. All three of these positive anomalies are larger in magnitude than any of the negative anomalies in the record, possibly due to the positively skewed nature of the snow accumulation rate distribution. The three longest integrated low snowfall periods are between AD 663–704, AD 933–975 and AD 1429–1468. The combination of the low snowfall period for AD 663–704 followed by the high snowfall period AD 727–783 results in a substantial trend in snow accumulation rate between the mid 7th to the end of the 8th century.

There is no obvious relationship between anomalous accumulation periods, or trends associated with them, and the the annually-dated volcanic history of Plummer et al. (2012), because it is unlikely that the low-pass filtered accumulation record would reflect the high frequency effect of atmospheric sulphate loading due to volcanic activity. Similarly, the 1000-year Law Dome CO_2 record of Rubino et al. (2013) shows no obvious commonalities between CO_2 and accumulation.

In contrast, spectral analysis of the 2 kyr annual snow accumulation rate record (Fig. 9) shows a number of significant periodicities in the sub-decadal band of 2.4–8.5 years, and one 29.7-year period is also evident, which may be related to climate variability. The sub-decadal power at 2.4–8.5 years is in the broad band of ENSO-type frequencies. An analysis of sea salts at Law Dome has previously shown an ENSO signal in the summer-period sea salts (Vance et al., 2013), so it is interesting to note that ENSO-type frequencies are also evident in the snow

accumulation rate record. Despite this, there is no significant correlation between the snow accumulation rate record presented here and the Southern Oscillation Index over the epoch AD 1870–2012. The 29.7-year period may be related to the IPO (Power et al., 1999), for which a 1000-year reconstruction has been produced recently using multiple Law Dome records (including snow accumulation rate) (Vance et al., 2014). The higher frequencies in the sub-decadal band (2.4 and 8.5 years) are generally more intermittent throughout the 2 kyr period (Fig. 10), probably due to noise associated with surface processes and the passage of sastrugi over the site. The 29.7-year period, in contrast, is more persistent throughout the record, and there are multi-centennial epochs where this frequency is quite strong (e.g. AD 100–550, AD 750–1000 and AD 1500–2012). This suggests (if this period is associated with the IPO) that the IPO signal has remained relatively steady at Law Dome for the past 2 kyr.

Comparing the spectral properties of the two different snow accumulation rate time-series (power law compared to piece-wise linear vertical strain rate models), revealed that there is less low frequency power in the power law model, which is consistent with removal of the concave bias in vertical strain rates from the the piece-wise linear model.

The snow accumulation rate history from the DSS ice-core captures broad scale variability across a large region of East Antarctica, well beyond the immediate vicinity of the Law Dome summit (see Fig. 11), indicated by the spatial coherence of annual snow accumulation rate correlation from two climate reanalysis models. Temporal correlations at Law Dome are significant for both ERA-Interim ($r = 0.6973$, $p < 0.001$) and RACMO2.1/ANT ($r = 0.7604$, $p < 0.001$). The spatial pattern of the correlation between the modelled snow accumulation rate at Law Dome and elsewhere in Antarctica agrees well between the two models, although there is a much larger region of significant positive correlation in Queen Maud Land, East Antarctica using the RACMO2.1/ANT dataset. The magnitudes of the annual snow accumulation rates are also in reasonable agreement. For the AD 1979–2012 period covered by ERA-Interim, the mean calculated snow accumulation rate is $0.749 \pm 0.142\,\mathrm{m\,yr^{-1}}$ ie compared

to the ERA-Interim modelled value of $0.713 \pm 0.136\,\mathrm{m\,yr^{-1}}$ ie. The comparison with RACMO2.1/ANT is over the period AD 1979–2010, where the calculated mean rate is $0.759 \pm 0.141\,\mathrm{m\,yr^{-1}}$ ie and the RACMO2.1/ANT mean value is $0.525 \pm 0.087\,\mathrm{m\,yr^{-1}}$ ie. It is worth noting that this is a predominantly positive/neutral IPO period and these
5 spatial relationships could change during strongly negative IPO periods given the clear IPO signal that is present at Law Dome (Vance et al., 2014).

The Law Dome regional accumulation map exhibits large scale spatial coherence Fig. 11, with an average *e*-folding distance of 900 km (distance at which the correlation drops to e^{-1}). This suggests that inter-annual variability in snowfall is dominated by
10 year to year changes in the large scale atmosphere dynamical forcing. van Ommen and Morgan (2010) previously reported a teleconnection pattern linking Law Dome accumulation with a zonal wave three index. The spatial correlation between 500 hPa geopotential height and the snow accumulation rate (Fig. 12) shows a quasi-ZW3 pattern, however the Australian and African high pressure poles are contracted
15 towards Antarctica. Principal component analysis (PC) of the Southern Hemisphere 500 hPa geopotential height field supports this. While PC1 (31 %) and PC2 (15 %) represent most of the dominant annular variability in the Southern Hemisphere 500 hPa geopotential height, in the Law Dome region there is little correlation between these first two components and accumulation. In contrast, PC3 shows a strong correlation with
20 Law Dome accumulation in the Law Dome region (Fig. 12 inset). This local modulation of the large scale variability may represent a tropical signal as demonstrated by the relationship between PC3 and the Pacific-South American modes (Mo and Paegle, 2001). This is a further line of evidence that Law Dome ice cores preserve tropical signals, and are not only sensitive to the dominant annular signal, which is centered
25 over West Antarctica (Vance et al., 2013, 2014).

Full Screen / Esc

Printer-friendly Version

Interactive Discussion

5 Conclusions

Two thousand years (AD −22 to AD 2012) of annual snow accumulation rates have been calculated for Law Dome, which extends the previous 750-year record. This study represents the first published account of data from a short ice core collected in the 2012–2013 austral summer (DSS1213), which has been used to extend an existing composite record from the site. To deconvolve the effects of ice sheet thinning on calculated snow accumulation rate profiles, two vertical strain rate models were evaluated, of which a power law model proved the most appropriate. The long-term accumulation rate of $0.688 \pm 0.130 \, \mathrm{m \, yr^{-1}}$ ie for this model is in agreement with previous estimates, and further supports the notion that there is no long-term trend in snow accumulation rates, or that any trend is constant and linear over the period of measurement. Several anomalous periods of accumulation exist in the record, most notably the periods of AD 380–442, AD 727–783 and AD 1970–2009 (high accumulation) and AD 663–704, AD 933–975 and AD 1429–1468 (low accumulation). The record has wide-reaching relevance, indicated by a spatial coherence in correlations with two climate reanalysis models showing the capture of large scale variability and possible links to tropical and higher-latitude dynamical forcing. Furthermore, significant periodicities were observed in the record which were broadly consistent with ENSO- and IPO-type variability, suggesting these patterns play an important role in the delivery of mass to the Law Dome region.

The Supplement related to this article is available online at doi:10.5194/cpd-10-4469-2014-supplement.

Research Centre (ACE CRC). ECMWF ERA-Interim data used in this study have been obtained from the ECMWF data server.

References

Abram, N. J., Mulvaney, R., Vimeux, F., Phipps, S. J., Turner, J., and England, M. H.: Evolution of the Southern Annular Mode during the past millennium, Nature Climate Change, 4, 1–6, doi:10.1038/NCLIMATE2235, 2014. 4471

Bamber, J. L., Gomez-Dans, J. L., and Griggs, J. A.: A new 1 km digital elevation model of the Antarctic derived from combined satellite radar and laser data – Part 1: Data and methods, The Cryosphere, 3, 101–111, doi:10.5194/tc-3-101-2009, 2009. 4486

D'Agostino, R., Belanger, A., and D'Agostino, Jr., R.: A suggestion for using powerful and informative tests of normality, Am. Stat., 44, 316–321, 1990. 4479

Dansgaard, W. and Johnsen, S.: A flow model and a time scale for the ice core from Camp Century, Greenland, J. Glaciol., 8, 215–223, 1969. 4474, 4475

Dee, D. P., Uppala, S. M., Simmons, A. J., Berrisford, P., Poli, P., Kobayashi, S., Andrae, U., Balmaseda, M. A., Balsamo, G., Bauer, P., Bechtold, P., Beljaars, A. C. M., van de Berg, L., Bidlot, J., Bormann, N., Delsol, C., Dragani, R., Fuentes, M., Geer, A. J., Haimberger, L., Healy, S. B., Hersbach, H., Hólm, E. V., Isaksen, L., Kållberg, P., Köhler, M., Matricardi, M., McNally, A. P., Monge-Sanz, B. M., Morcrette, J.-J., Park, B.-K., Peubey, C., de Rosnay, P., Tavolato, C., Thépaut, J.-N., and Vitart, F.: The ERA-Interim reanalysis: configuration and performance of the data assimilation system, Q. J. Roy. Meteor. Soc., 137, 553–597, doi:10.1002/qj.828, 2011. 4496, 4497

Ghil, M., Allen, M. R., Dettinger, M. D., Ide, K., Kondrashov, D., Mann, M. E., Robertson, A. W., Saunders, A., Tian, Y., Varadi, F., and Yiou, P.: Advanced spectral methods for climatic time series, Rev. Geophys., 40, 41 pp. doi:10.1029/2001RG000092, 2002. 4494

Hutter, K.: Dynamics of glaciers and large ice masses, Annu. Rev. Fluid Mech., 87–130, 1982. 4476

Lenaerts, J. T. M., van den Broeke, M. R., van de Berg, W. J., van Meijgaard, E., and Kuipers Munneke, P.: A new, high-resolution surface mass balance map of Antarctica (1979–2010) based on regional atmospheric climate modeling, Geophys. Res. Lett., 39, 1–5, doi:10.1029/2011GL050713, 2012. 4496

Law Dome accumulation

J. Roberts et al.

Title Page

Abstract | Introduction

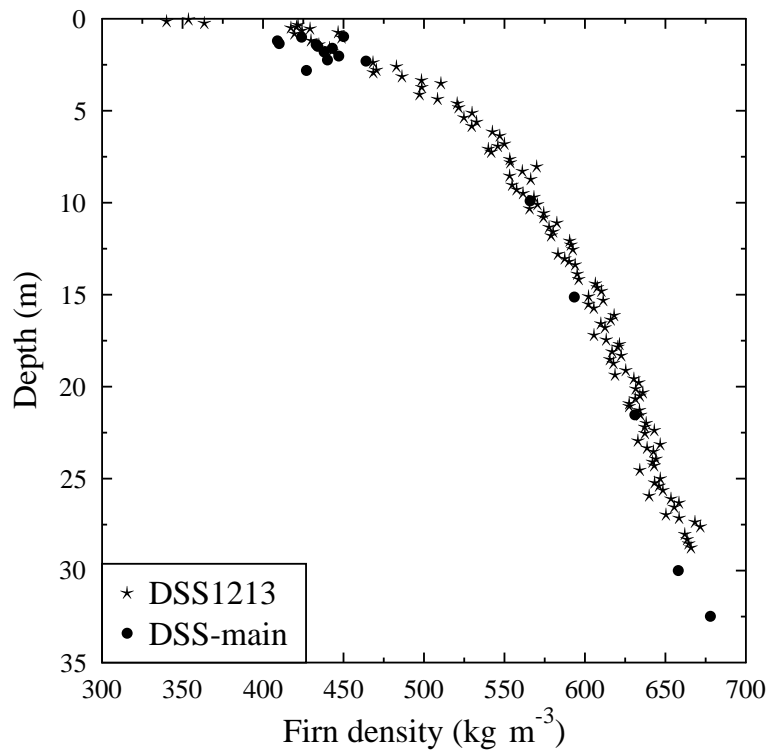Conclusions | References

Tables | Figures

◀ | ▶

◀ | ▶

Back | Close

Full Screen / Esc

Printer-friendly Version

Interactive Discussion

Lliboutry, L. A.: A critical review of analytical approximate solutions for steady state velocities and temperature in cold ice sheets, Zeitschift fur Gletscherkunde und Glazialgeologie, 15, 135–148, 1979. 4474, 4475

Mo, K. C. and Paegle, J. N.: The Pacific-South American modes and their downstream effects, Int. J. Climatol., 21, 1211–1229, doi:10.1002/joc.685, 2001. 4481

Morgan, V., Wookey, C., Li, J., van Ommen, T., Skinner, W., and Fitzpatrick, M.: Site information and initial results from deep ice drilling on Law Dome, Antarctica, J. Glaciol., 43, 3–10, 1997. 4471, 4474, 4478

Morgan, V., van Ommen, T., Elcheikh, A., and Jun, L.: Variations in shear deformation rate with depth at Dome Summit South, Law Dome, East Antarctica, Ann. Glaciol., 27, 135–139, 1998. 4475, 4476, 4477, 4478, 4490

Patterson, W.: The Physics of Glaciers, 3rd edn., Butterworth Heinemann, Oxford, 1994. 4473, 4475

Plummer, C. T., Curran, M. A. J., van Ommen, T D., Rasmussen, S. O., Moy, A. D., Vance, T. R., Clausen, H. B., Vinther, B. M., and Mayewski, P. A.: An independently dated 2000 yr volcanic record from Law Dome, East Antarctica, including a new perspective on the dating of the 1450s CE eruption of Kuwae, Vanuatu, Clim. Past, 8, 1929–1940, doi:10.5194/cp-8-1929-2012, 2012. 4472, 4473, 4479

Power, S., Casey, T., Folland, C., Colman, A., and Mehta, V.: Inter-decadal modulation of the impact of ENSO on Australia, Clim. Dynam., 15, 319–324, 1999. 4480

Raphael, M. N.: A zonal wave 3 index for the Southern Hemisphere, Geophys. Res. Lett., 31, L23212, doi:10.1029/2004GL020365, 2004. 4472

Roberts, J. L., Warner, R. C., Young, D., Wright, A., van Ommen, T. D., Blankenship, D. D., Siegert, M., Young, N. W., Tabacco, I. E., Forieri, A., Passerini, A., Zirizzotti, A., and Frezzotti, M.: Refined broad-scale sub-glacial morphology of Aurora Subglacial Basin, East Antarctica derived by an ice-dynamics-based interpolation scheme, The Cryosphere, 5, 551–560, doi:10.5194/tc-5-551-2011, 2011. 4471

Rubino, M., Etheridge, D. M., Trudinger, C. M., Allison, C. E., Battle, M. O., Langenfelds, R. L., Steele, L. P., Curran, M., Bender, M., White, J. W. C., Jenk, T. M., Blunier, T., and Francey, R. J.: A revised 1000 y atmospheric δ^{13}C-CO$_2$ record from Law Dome and South Pole, Antarctica, J. Geophys. Res.-Atmos., 118, 8482–8499, doi:10.1002/jgrd.50668, 2013. 4479

Title Page

Abstract · Introduction

Conclusions · References

Tables · Figures

◄◄ · ►►

◄ · ►

Back · Close

Full Screen / Esc

Printer-friendly Version

Interactive Discussion

van Ommen, T. D. and Morgan, V.: Calibrating the ice core paleothermometer using seasonality, J. Geophys. Res., 102, 9351–9357, doi:10.1029/96JD04014, 1997. 4473

van Ommen, T. D. and Morgan, V.: Snowfall increase in coastal East Antarctica linked with southwest Western Australian drought, Nat. Geosci., 3, 267–272, doi:10.1038/ngeo761, 2010. 4472, 4478, 4481

van Ommen, T. D., Morgan, V., and Curran, M. A. J.: Deglacial and Holocene changes in accumulation at Law Dome, East Antarctica, Ann. Glaciol., 39, 359–365, doi:10.3189/172756404781814221, 2004. 4471, 4473, 4478

Vance, T., Roberts, J., Plummer, C., Kiem, A., and van Ommen, T.: Interdecadal Pacific variability and eastern Australian mega-droughts over the last millennium, Geophys. Res. Lett., submitted, 2014. 4471, 4480, 4481

Vance, T. R., van Ommen, T. D., Curran, M. A. J., Plummer, C. T., and Moy, A. D.: A millennial proxy record of ENSO and Eastern Australian rainfall from the Law Dome Ice Core, East Antarctica, J. Climate, 26, 710–725, doi:10.1175/JCLI-D-12-00003.1, 2013. 4471, 4472, 4479, 4481
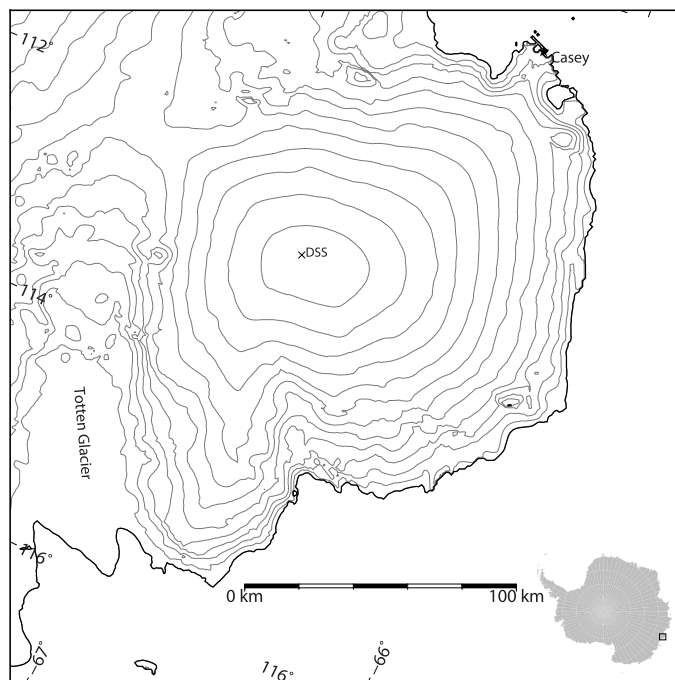
Figure 1. Law Dome, East Antarctica and the location of the Dome Summit South (DSS) borehole. Also shown are 100 m surface elevation contours from Bamber et al. (2009).

Figure 2. Firn density from the DSS-main and DSS1213 ice cores.

Full Screen / Esc

Printer-friendly Version

Interactive Discussion
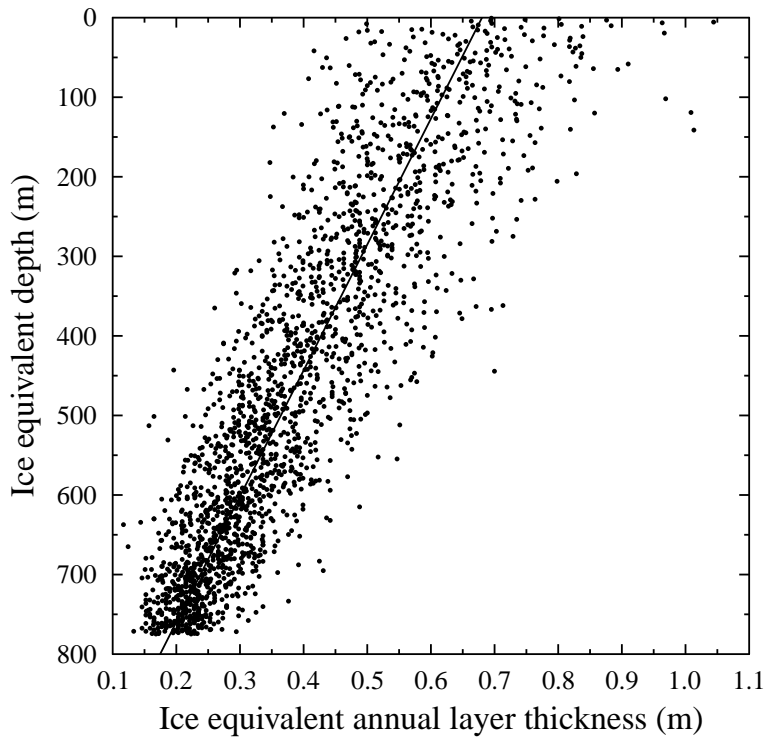
Figure 3. Piece-wise linear fit to the annual layer thickness data.

Full Screen / Esc

Printer-friendly Version

Interactive Discussion
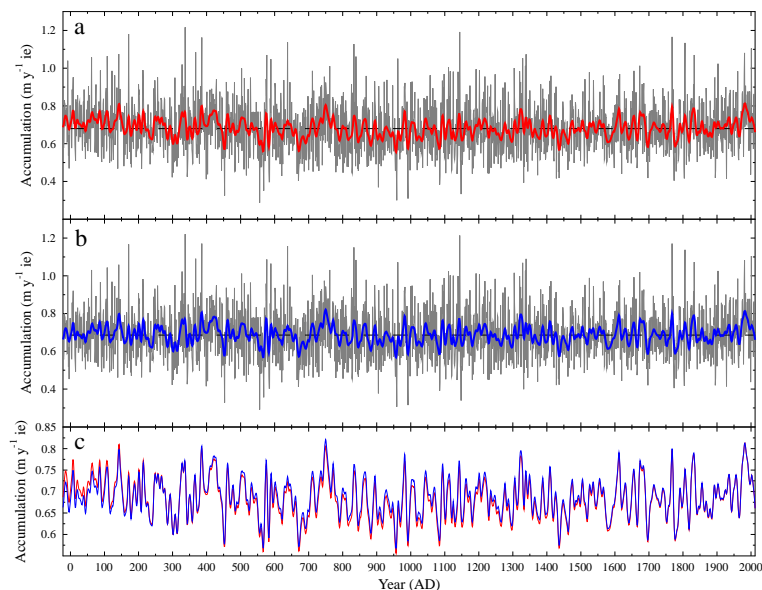
Figure 4. Annual (grey) and smoothed (coloured) snow accumulation rate history for AD −22–2012 based on **(a)** piece-wise linear vertical strain rate profile, with the long-term average snow accumulation rate of $0.680\,\mathrm{m\,yr^{-1}}$ ie shown (dashed horizontal), **(b)** power law vertical strain rate profile, with the long-term average snow accumulation rate of $0.686\,\mathrm{m\,yr^{-1}}$ ie shown (dashed horizontal) and **(c)** smoothed piece-wise linear (red) and power law (blue) snow accumulation histories. Note the changed vertical scale to highlight the similarities of the two smoothed records.
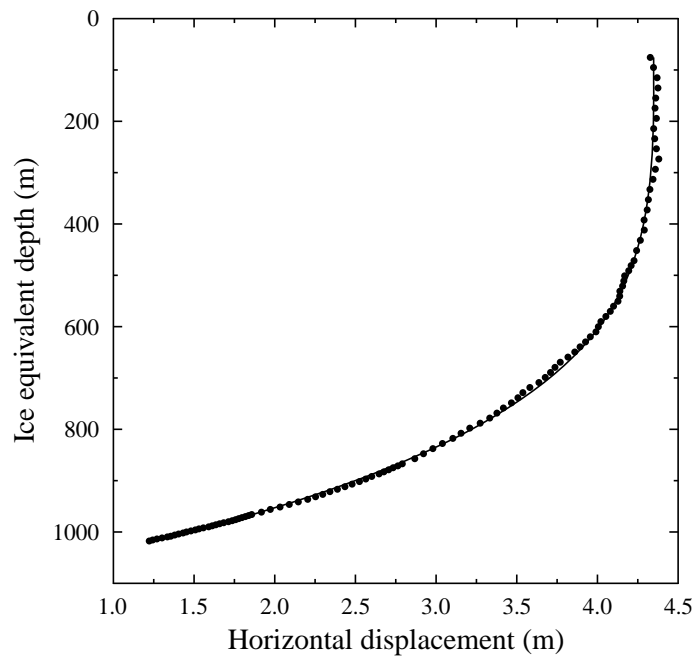
Figure 5. Power law velocity profile fit (line) to the horizontal displacement data (dots) of Morgan et al. (1998).
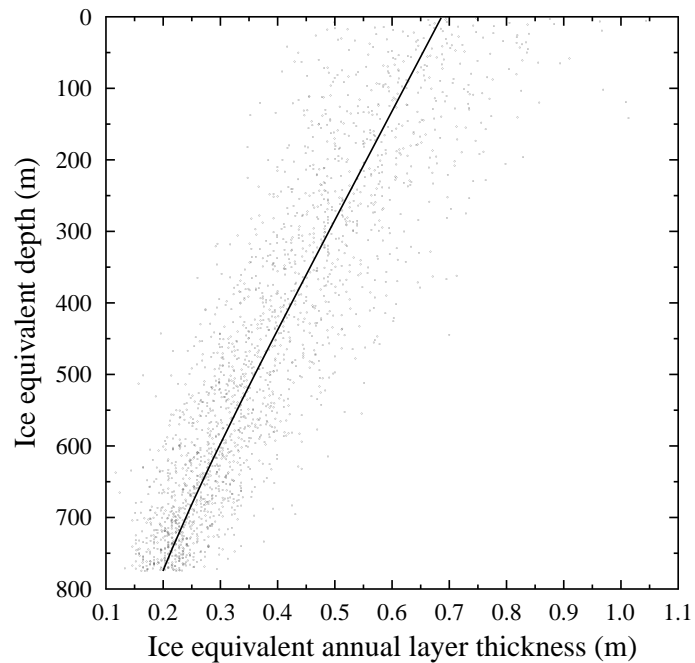
Figure 6. Power law fit to the annual layer thickness data.
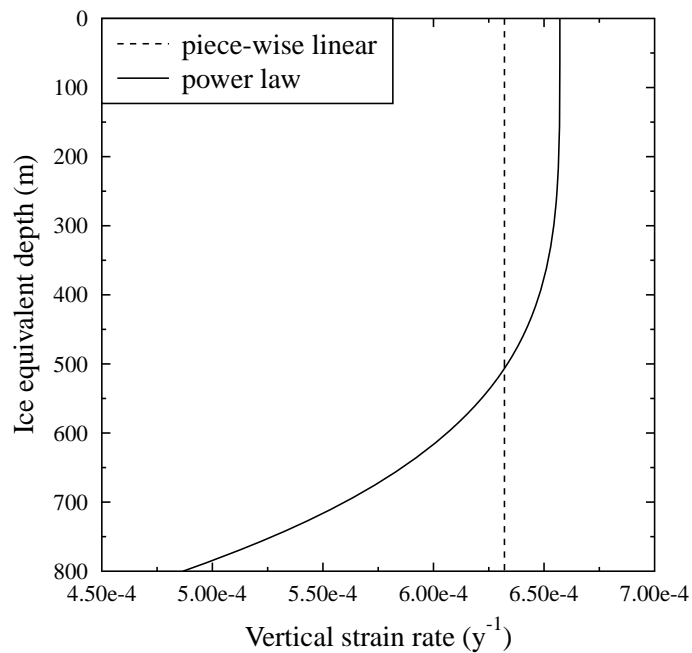
Figure 7. Vertical strain rates from piece-wise linear and power law models to the annual layer thickness data.
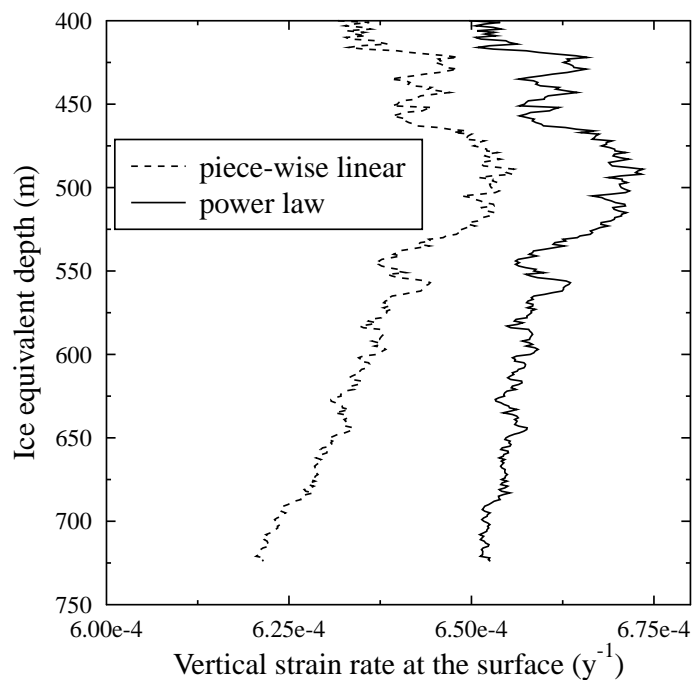
Figure 8. Surface vertical strain rates from piece-wise linear and power law models to the annual layer thickness data using a 100 m moving window of depth data and a fixed long-term average annual snow accumulation rate.
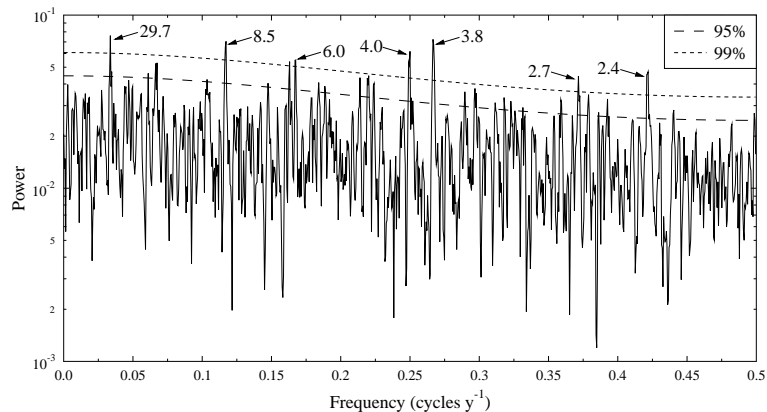
Figure 9. MultiTaper Method power spectrum (Ghil et al., 2002) of snow accumulation rate time series using a resolution of 2 and 3 tapers of power law based construction. Period of spectral components above 99 % significant shown.
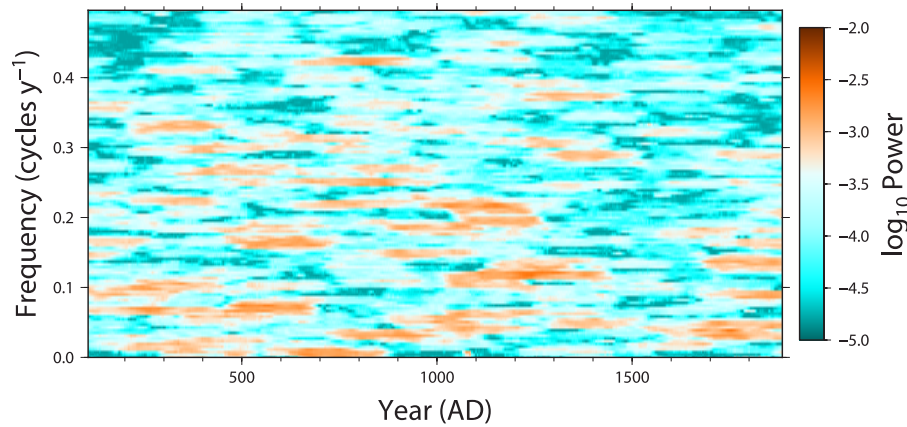
Figure 10. MultiTaper Method evolutive power spectrum of power law snow accumulation rate time series using a resolution of 2, 3 tapers and a bandwidth of 256 years.
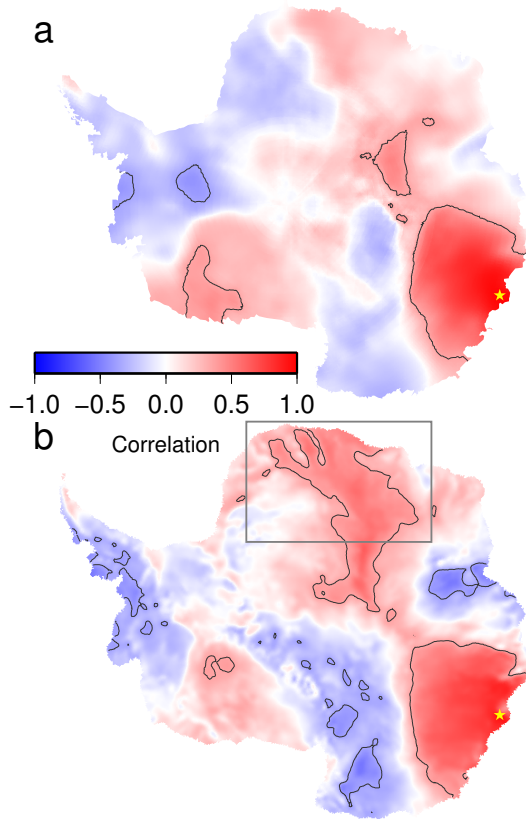
Figure 11. Spatial correlation maps for **(a)** ERA-Interim precipitation-evaporation (Dee et al., 2011) for AD 1979–2013 and **(b)** RACMO2.1/ANT surface mass balance (Lenaerts et al., 2012) AD 1979–2010. Contour shows the 95 % confidence level while yellow stars denote the location of DSS and the grey box shows Queen Maud Land.
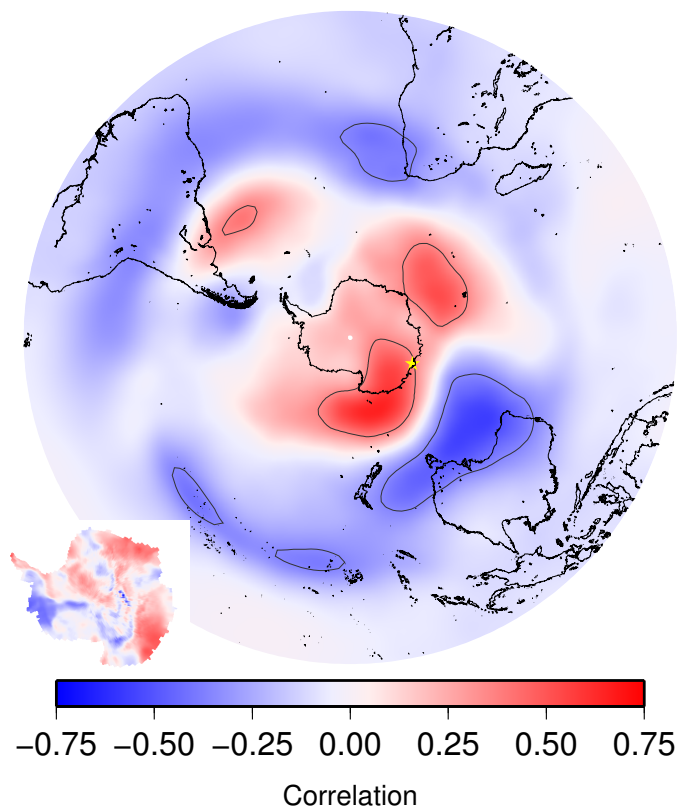
Figure 12. Spatial correlation map for ERA-Interim 500 hPa geopotential height (Dee et al., 2011) and power-law based snow accumulation rate for AD 1979–2012. Contour shows the 95 % confidence level while yellow star denotes the location of DSS. Inset: third PC of Southern Hemisphere 500 hPa geopotential height correlated with power-law based snow accumulation rate for AD 1979–2012.